Journal of Inorganic and Organometallic Polymers and Materials (2021) 31:3505–3524
https://doi.org/10.1007/s10904-021-01976-5

Responsibility of Bi_2O_3 Content in Photon, Alpha, Proton, Fast and Thermal Neutron Shielding Capacity and Elastic Moduli of ZnO/B_2O_3/Bi_2O_3 Glasses

Y. S. Rammah[1] · F. I. El-Agawany[1] · A. Gamal[1] · I. O. Olarinoye[2] · Emad M. Ahmed[3] · A. S. Abouhaswa[1,4]

Received: 16 January 2021 / Accepted: 16 March 2021 / Published online: 27 March 2021

Abstract
The effect of Bi_2O_3 content on photon, alpha particle, proton, fast and thermal neutron shielding capacity, and elastic moduli of 10ZnO-(90-x)B_2O_3-xBi_2O_3 (ZBB-glasses): x = 25–50 mol% has been investigated. The mass density and Bi-content of the ZBB-glasses had the greatest impact on the values of mass and linear attenuation coefficients. The mass and linear attenuation coefficients values were followed the trend $(ZBB25)_{MAC,LAC} < (ZBB30)_{MAC,LAC} < (ZBB35)_{MAC,LAC} < (ZBB40)_{MAC,LAC} < (ZBB45)_{MAC,LAC} < (ZBB50)_{MAC,LAC}$. The mean free path (MFP) and half value layer (HVL) were having the same trend and opposite to which obtained in mass and linear attenuation coefficients. All the ZBB-glasses showed almost similar charged particle shielding capacity. However, ZBB50 had a comparable charged particle absorption efficiency. There was a 57% growth in fast neutron removal cross section as Bi_2O_3 molar concentration increased to 50% in the ZBB-glass matrix. ZBB50 possesses the highest fast neutron removal cross section among the ZBB-glasses. In terms of thermal neutron absorbing capacity, the presence of B in the glass matrix ensures that the ZBB-glasses are good thermal neutron absorption. ZBB25 has the highest thermal neutron absorption capacity among the investigated glasses. Generally, ZBB-glasses can be adopted for photon, thermal neutron, proton, and alpha particle shielding purposes. In addition, elastic (shear, longitudinal, and Young's) moduli and Poisson's ratio are changed significantly with the increase of Bi_2O_3 content mol% in ZBB-glasses.

Keywords Glass · Photon · Elastic moduli · Shielding capacity · Thermal neutron

1 Introduction

The use of ionizing radiation in various fields has continued to grow as science and technology have advanced [1–10]. As a result, the sources of man-made radiation exposure to humans and the environment have increased. The dangers of exposing biota and living tissues to ionizing radiation from various sources, forms, and energies are well understood. [11]. Some radiation—induced effects in human tissues are deterministic while others are stochastic all of which may constitute health hazards [11]. Radiation protection has thus become an important doctrine in all peaceful uses of nuclear/atomic radiations from various sources. The cardinal objective of any radiation protection protocol is to eliminate deterministic effects and reduce the chances of stochastic effects to the barest minimum in all biological systems [5–11]. Protection from radiation via the use of a radiation shield is one of the effective ways of achieving these [1–10, 12–14].

Traditional shielding materials are sometimes costly, bulky, non-durable, toxic, having unstable chemical, mechanical, and ultimately shielding properties. On the contrary, advanced radiation protection protocols are required in the modern application of radiation need materials that are non-toxic, durable, environmentally friendly, and durable [5–10, 12–14]. Glass is a class of material that fits into this category of materials. Glasses may be used for shielding in the medical diagnostic and therapeutic application of radiation, storing, and transporting the nuclear waste of any level,

✉ Y. S. Rammah
dr_yasser1974@yahoo.com

[1] Department of Physics, Faculty of Science, Menoufia University, Shebin El Koom 32511, Egypt

[2] Department of Physics, School of Physical Sciences, Federal University of Technology, Minna, Nigeria

[3] Department of Physics, College of Science, Taif University, P.O. Box 11099, Taif 21944, Saudi Arabia

[4] Ural Federal University, 19 Mira St, 620002 Yekaterinburg, Russia

high energy nuclear research, space explorations, and many more areas of radiation applications [12–17].

Glass is one of the most and important materials with different applications in human society. This is partly due to its ease of production, and ability to be shaped into several geometries [1–10, 12–17]. Thus, in the past, many products have been produced from a glass of diverse compositions and properties. The most traditional applications of glasses include optical devices, household items, ornaments, decorative, and building materials. Technological development has expanded the use of glass in areas such as telecommunication, photonics, and many more [17–21].

Recent advances in glass research have suggested that some glass compositions with good radiation shielding properties can be produced and used for radiation shielding [1–10, 15–21]. While some of these studies have produced glasses, which are currently available for shielding purposes, many more glasses are still being investigated. It has been proven that one of the ways to improve the radiation shielding capacity and some optical properties of a glass system is to include a heavy metal oxide such as Bi_2O_3 in its composition [3, 22–24]. In 2017, El Bashir et al. [25] showed that increasing the Bi_2O_3 content of the BaO- Bi_2O_3-P_2O_3 glass system increased the mass density and elastic moduli of the glass system while decreasing the molar volume. It was also confirmed through calculated photon interaction parameters such as a half-value layer, effective atomic number, and exposure buildup factors that the photon shielding capacity of the glass system improved with an increase in Bi_2O_3 content. Also, the gamma shielding capacity of the Te-Bi_2O_3-B_2O_3-ZnO glass system was improved when the Bi_2O_3 content was increased [23]. Higher refractive indices coupled with enhanced radiation shielding features have been reported for B_2O_3- Bi_2O_3-CaO-Na_2O glass system containing higher concentrations of Bi_2O_3 [22]. Similar positively linear correlations between Bi_2O_3 content and photon, proton, and alpha particle shielding efficiency of B_2O_3- Bi_2O_3, TeO_2-V_2O_5-Bi_2O_3, and Al_2O_3-Na_2O- B_2O_3-Bi_2O_3 glass systems [26, 27]. These findings and many more have revealed that the inclusion of Bi_2O_3 could have a positive impact on the radiation shielding capacity of any glass system. To this end, from the literature on can conclude that Bi_2O_3 has a positive effect to enhance the physical properties like density, mechanical properties, optical properties to be applicable in optoelectronic devices, solid state lasers, thermal sensors, and optical fiber amplifiers. As well as being applicable in radiation protection applications to help workers in radiation fields from radiation exposure hazards [15–24].

Consequently, in this research, we investigate the role of Bi_2O_3 content in elastic moduli, gamma-ray, alpha particles, protons, fast, and thermal neutron shielding capacity of 10ZnO-(90-x)B_2O_3-xBi_2O_3 (ZBB) glasses.

2 Materials and Calculations

2.1 Materials

Six glass samples of zinc bismuth-borate of form 10ZnO-(90-x)B_2O_3-xBi_2O_3 namely as ZBB-glasses and x = 25–50 mol% were selected from Ref. [28]. Generally, the selected glasses were labeled as S-glasses and individually as:

ZBB25: 10ZnO-65B_2O_3-25Bi_2O_3 mol%, **ZBB30:** 10ZnO-60B_2O_3-30Bi_2O_3 mol%, **ZBB35:** 10ZnO-55B_2O_3-35Bi_2O_3 mol%, **ZBB40:** 10ZnO-50B_2O_3-40Bi_2O_3 mol%, **ZBB45:** 10ZnO-45B_2O_3-45Bi_2O_3 mol%, and **ZBB50:** 10ZnO-40B_2O_3-50Bi_2O_3 mol%. Samples code, compositions, density, and molar volume of ZBB-glasses are tabulated in Table 1.

2.2 Radiation Shielding Parameters

2.2.1 Photons

Generally, photons (x- and gamma-rays) transmission in narrow beam geometry through an interacting medium of thickness t is described via the Beer-Lambert law as:

$$X = X_o e^{-\mu t} \tag{1}$$

where, X_o, X, and μ is the photon measurable transmission/interaction quantity before and after emerging from the

Table 1 Code, chemical composition, density, and molar volume of the 10ZnO-(90-x)B_2O_3-xBi_2O_3:(ZBB): x = 25–50 mol% glasses

Sample code	Composition (mol%)			Density, ρ (g/cm^3) ± 0.001	Molar volume, V_m (cm^3/mol) ± 0.01
	ZnO	B_2O_3	Bi_2O_3		
ZBB25	10	65	25	4.265	39.83
ZBB30	10	60	30	4.468	42.45
ZBB35	10	55	35	4.675	44.81
ZBB40	10	50	40	4.972	46.12
ZBB45	10	45	45	5.213	47.79
ZBB50	10	45	50	5.313	50.62

interacting medium, and the linear attenuation coefficient of the medium, respectively. the transmission quantity X may be intensity, energy, particle fluxes/ fluence, absorbed dose or exposure. The linear attenuation coefficient (LAC) expresses the flux of the photons that emerge from the absorber without interaction. It is a quantity that can thus be used to measure the photon shielding capability of an attenuating medium. Other parameters that can be used to express the photon interaction capacity of a material include: the mass attenuation coefficient (MAC, μ_m), half-value layer (HVT), mean free path (MFP), and the effective atomic number (Z_{eff}). They are all derivable from LAC according to the expressions [29]:

$$\mu_m = \frac{\mu}{\rho} \tag{2}$$

$$HVL = {}^{ln2}/_{\mu} \tag{3}$$

$$MFP = {}^{1}/_{\mu} \tag{4}$$

$$Z_{eff} = \frac{\sum_i w_i A_i (\mu_m)_i}{\sum_i w_i \frac{A_i}{Z_i} (\mu_m)_i} \tag{5}$$

where, w_i, Z_i, and A_i in Eq. (5) represents the weight fraction, atomic and mass number of elemental *ith* component of the absorbing material.

MAC values of ZBB-glasses were estimated in this study via the use of WinXCOM [30] for a standard photon energy grid between 15 keV and 15 MeV. The calculated MAC values were used to estimate LAC, HVT, MFP and Z_{eff} of the glasses using Eqs. (2–5), respectively.

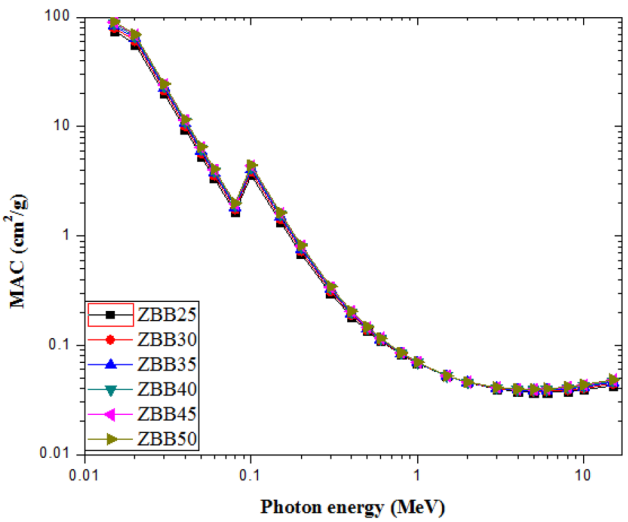

Fig. 1 MAC of ZBB-glasses as function of photon energy

In broad beam geometry, transmitted photon flux consists of uncollided (primary) and scattered (secondary) radiations. In such a scenario, the Beer-Lambert law (Eq. 1) is adjusted to accommodate the contribution of the secondary flux. Thus:

$$X = X_o B_X e^{-\mu t} \tag{6}$$

where, B_X is the photon buildup factor of the radiation quantity X. B_X is a non-dimensional adjustment parameter that is equal to unity in the narrow beam transmission geometry. A detailed discussion about B_X and the different methods of calculating them have been presented elsewhere [31–33]. For shielding calculations, B_X is the most practical use to evaluate the transmission factor that is defined from Eqs. (1) and (6) as:

$$(TF)_X = B_X e^{-\mu t} = e^{-\mu' t} \tag{7}$$

here

$$\mu'(\mu t) = \mu - \frac{lnB_X}{t} \tag{8}$$

and μ' is called the effective linear attenuation coefficient [34]. The exposure and energy absorption buildup factors of the glasses in the present study were calculated via the Phy-X/PSD software [33].

2.2.2 Neutrons

The interaction of neutrons with any medium produces three types of neutrons depending on the energy of the neutrons and the nature of the interacting material. These are transmitted, absorbed, and scattered neutron. The transmitted neutron escapes interaction, while the scattered and absorbed neutrons are scattered within the medium and absorbed via different neutron capturing processes. The statistical possibility that one or more of these processes occur is through the microscopic cross section of the reaction. On the other hand, the total (macroscopic) cross section of a neutron type is the sum of all interaction probabilities of such neutrons. The fast neutron removal cross section ($FNRC - \Sigma_R$) is the macroscopic cross section for fast neutrons having energies between 2 and 12 MeV. *FNRC* is almost a constant in this energy range and can be calculated via the equation [35]:

$$\Sigma_R = \rho \sum w_i \left(\frac{\Sigma_R}{\rho}\right)_i \tag{9}$$

where, ρ, w_i, and $\left(\frac{\Sigma_R}{\rho}\right)_i$ is the mass density of the interacting medium, weight fraction, and mass removal cross section of

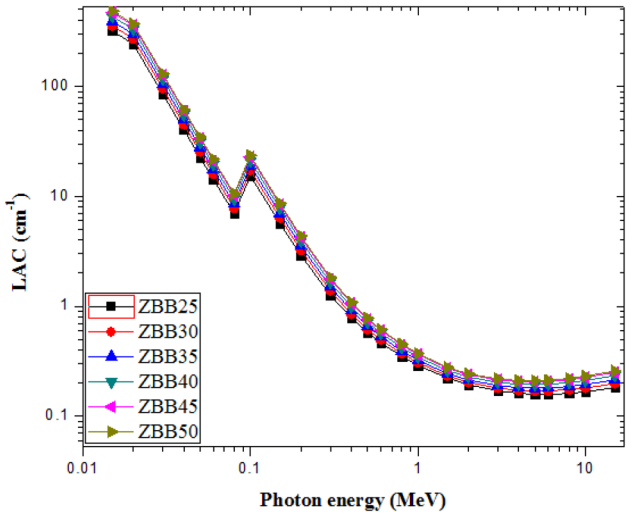

Fig. 2 Changes in LAC values of ZBB-glasses as function of photon energy

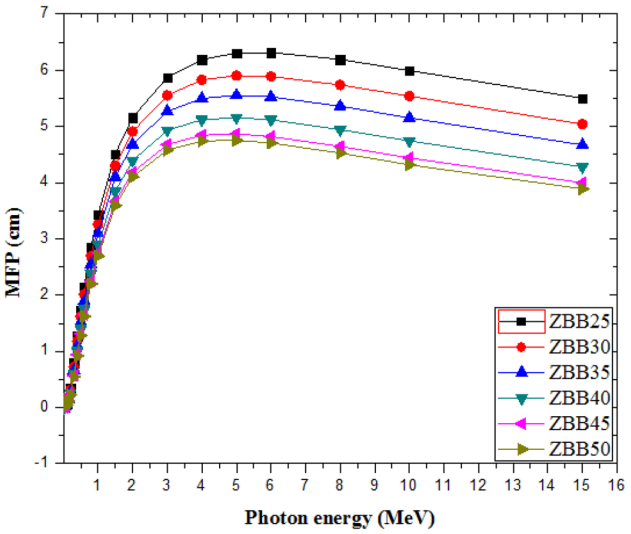

Fig. 3 Variation of MFP with photon energy for ZBB-glasses

the i^{th} element in it. $\frac{\Sigma_R}{\rho}$ of constituent element of any medium can be estimated via their respective atomic numbers, Z as:

$$\frac{\Sigma_R}{\rho} = 0.19Z^{-0.743} \quad \text{for } Z \leq 8; \tag{10}$$

and,

$$\frac{\Sigma_R}{\rho} = 0.125Z^{-0.565} \quad \text{for } Z > 8 \tag{11}$$

For thermal neutrons (with the energy of 25.30 MeV at the ambient temperature of 300 K), the total macroscopic

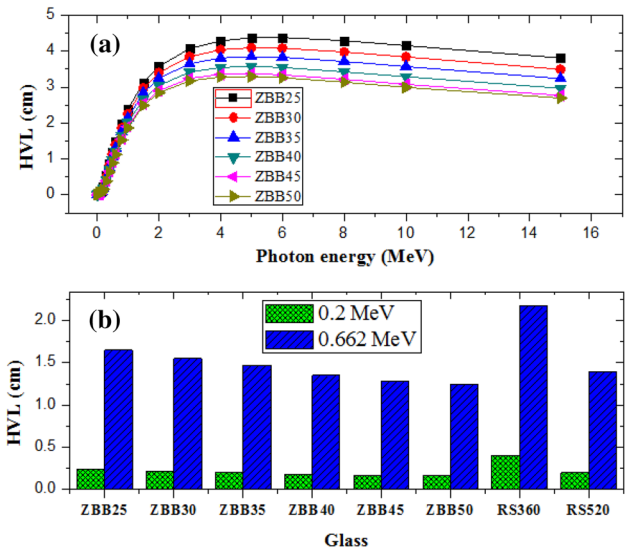

Fig. 4 **a** HVL as function of energy for the glasses and **b** compared with commercial shielding glasses at 0.2 and 0.662 MeV

cross-section Σ_T (cm^{-1}) of a medium may be calculated through the equation [36–38]:

$$\Sigma_T = 6.02 \times 10^{23} \rho \sum_i \frac{w_i}{M_i} (\sigma_T)_i \tag{12}$$

where, σ_T (cm^2) is the total microscopic cross section for scattering and absorption. Σ_R and Σ_T were calculated for the ZBB-glasses using Eqs. (9–12).

2.2.3 Proton and Alpha Particle

Total Mass Stopping Powers (TMSP) and projected range (R) of proton and alpha particles in ZBB-glasses were evaluated using SRIM-2013 software [39].

2.3 Elastic Moduli Calculations

In the current work, bulk, Young's, shear, longitudinal elastic moduli, and Poisson's ratio of the proposed ZBB-glasses were calculated via Makishima-Mackenzie (M-M) and bond compression (B-C) models [40–42]. The applied and used parameters for calculation processes for both two models are gathered and tabulated in Tables 4, 5, 6.

3 Results and Discussion

3.1 Radiation Shielding Competence

3.1.1 MAC, LAC, MFP, and HVL of ZBB-Glasses

The mass attenuation coefficient (MAC) spectra of ZBB-glasses represented as functions of photon energy in the

range of 0.015 to 15 MeV are shown in Fig. 1. The result showed that the MAC similarly varies with energy in all the glasses. It was observed that MAC values were highest at the least energy and decreased drastically as energy increased for energies below 0.8 MeV except at 0.1 MeV where a high sharp peak was noticed at this energy value. The peak is related to the K-x-ray absorption edge of the Bi atom forming the glass matrix. The sharp decrease in MAC values at the lowest energy zone is interpreted due to the dominance of the photoelectric absorption coefficient (PAC). The PAC generally decreased with the third or fourth power of the photon's average energy. Beyond 800 keV, the decrease in MAC becomes less rapid up to an energy of 6 MeV beyond which the MAC values of the glasses start to increase steadily. The slow decrease in MAC is attributed to Compton scattering absorption process. Photons are lost to Compton scattering process via inelastic collision of a photon with the free electrons in the interaction medium. The Compton interaction absorption is inversely proportional to photon energy. This explains why the decrease in MAC values is less rapid compared to energies less than 600 keV. At 6 MeV, the pair production absorption process takes place and dominates the behavior of the mass attenuation cross section. The total pair production cross section has a threshold energy of 1.022 MeV, then increases with photon energy and becomes significant at energies beyond 10 MeV [34]. This trend discussed the gradual increase in MAC as photon energy goes beyond 6 MeV. Comparing the MAC values

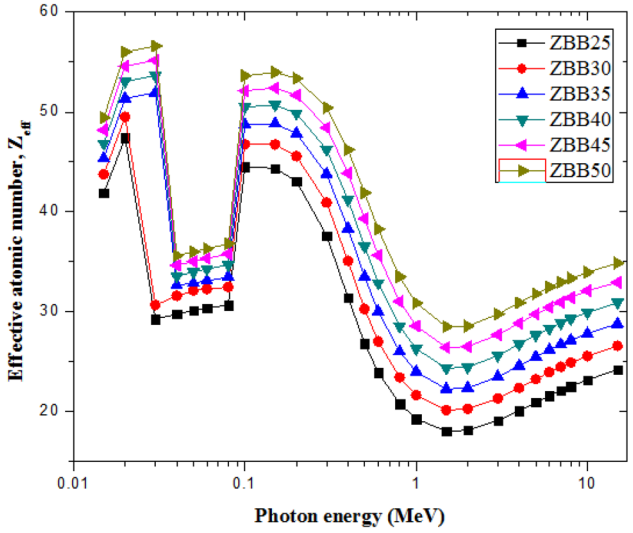

Fig. 5 Values of Z_{eff} for ZBB-glasses in relation to photon energy

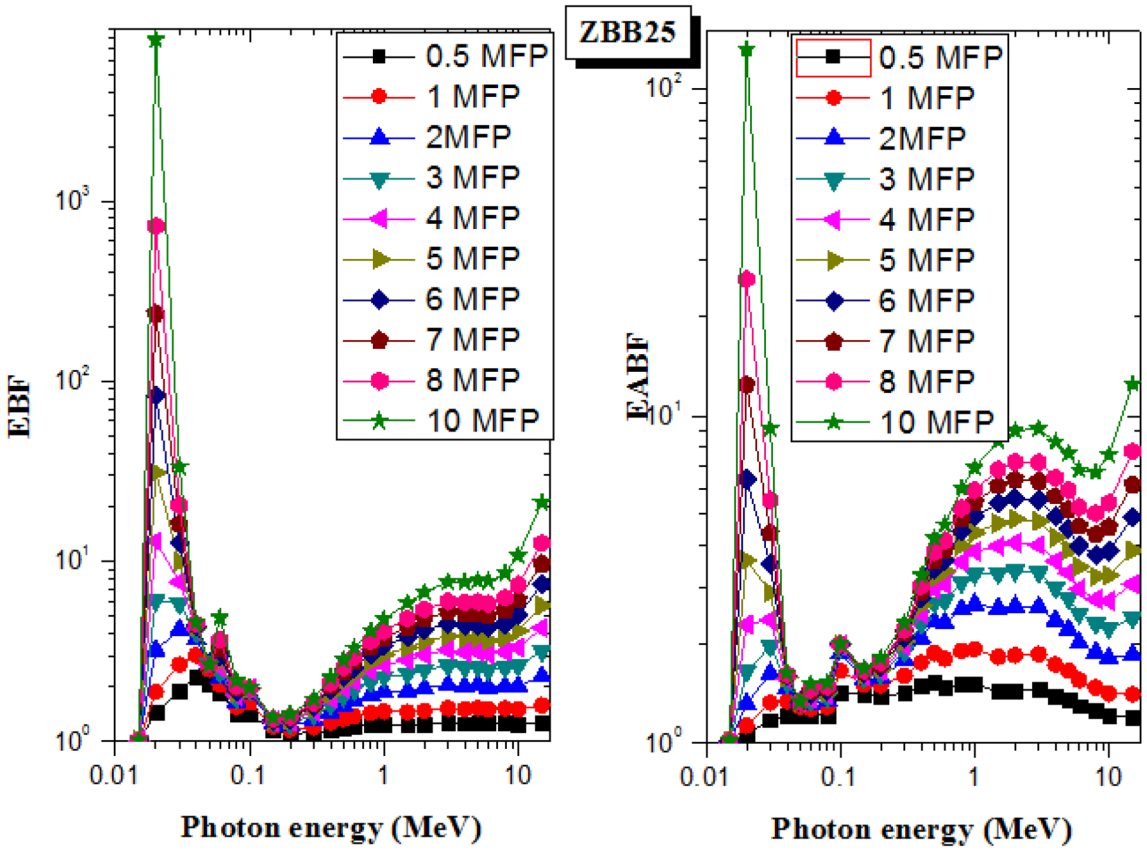

Fig. 6 EBF and EABF as functions of photon energy for ZBB25 glass sample

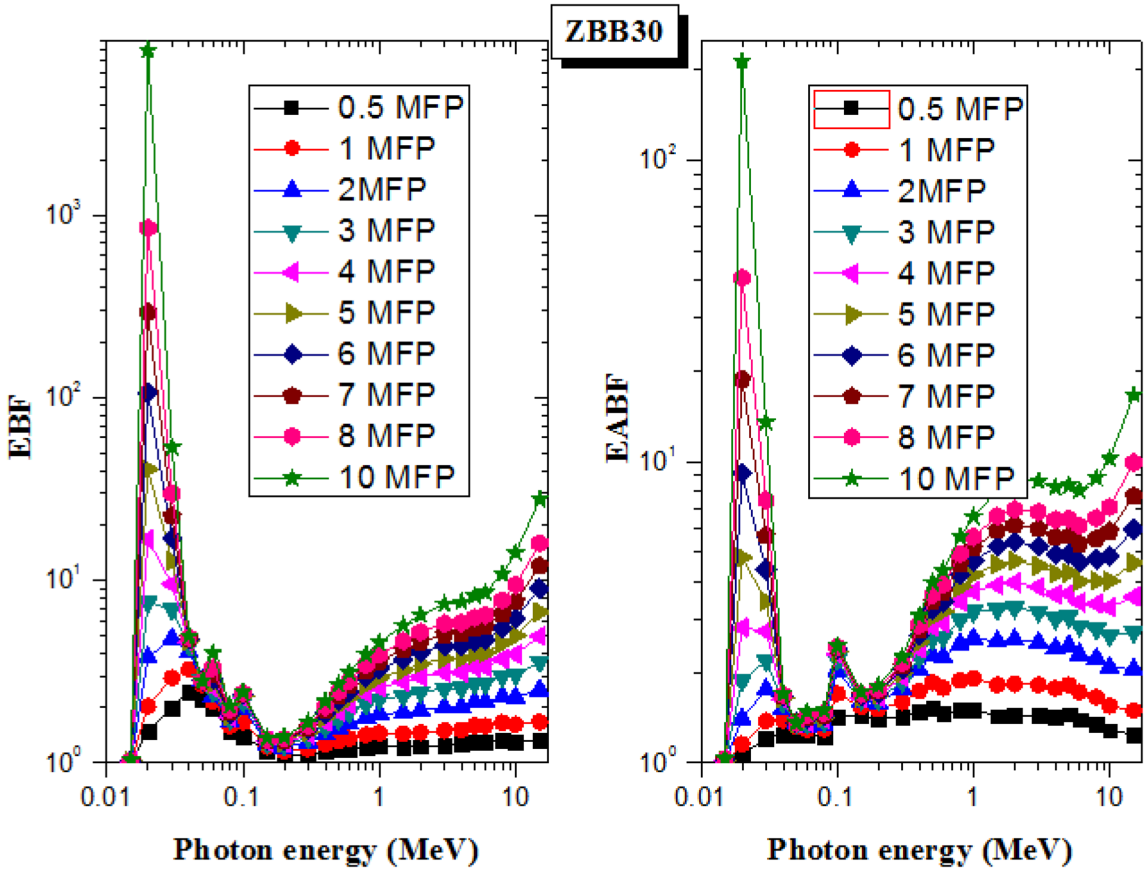

Fig. 7 EBF and EABF as functions of photon energy for ZBB30 glass sample

of the ZBB-glasses with one another, it could be observed that the values are close throughout the energy spectrum. However, MAC values increased at each energy following the order: ZBB25 < ZBB30 < ZBB35 < ZBB40 < ZBB45 < ZBB50. The maximum (minimum) values of MAC obtained at energy of 15 keV (6 MeV) respectively were 75 (0.0373), 79.9 (0.0379), 83.9 (0.0385), 87.2 (0.039), 90 (0.0394), and 91.2 (0.0396) $cm^2\ g^{-1}$ for ZBB25, ZBB30, ZBB35, ZBB40, ZBB45, and ZBB50, respectively. This order follows that of the mass density and Bi_2O_3 content of the glasses as given in Table 1. This shows that the mass attenuation coefficient of the glasses is closely linked with their mass density and chemical composition. The presence and increase in the content of a denser heavy metal oxide with superior MAC values ensured that glasses with a higher concentration of Bi_2O_3 improve the photon absorption capacity of the glasses. This trend has been reported in other glass matrices previously [3, 22–27].

The linear attenuation coefficients (LAC) values of ZBB-glasses as functions of photon energy are shown in Fig. 2. According to the result, LAC similarly varied with energy as the MAC. Thence, maximum LAC values were obtained at photon energy of 15 keV with values of 320, 357, 392, 434, 469, and 485 cm^{-1}, while the minimum values obtained at 6 MeV were 0.158, 0.17, 0.181, 0.95, 0.207 and 0.213 cm^{-1} for ZBB25, ZBB30, ZBB35, ZBB40, ZBB45, and ZBB50, respectively. The result also showed that the differences between LAC values of the glasses at each energy are more pronounced in contrast to those of MAC. This is due to the

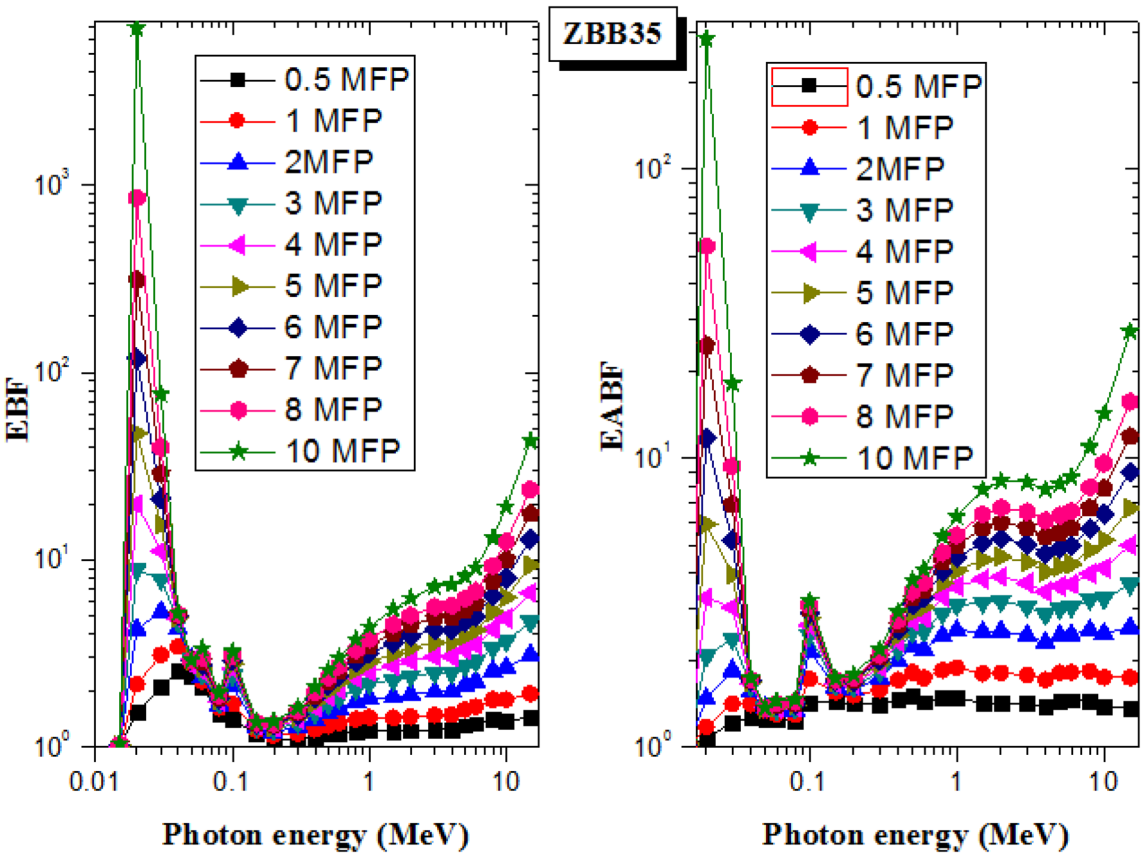

Fig. 8 EBF and EABF as functions of photon energy for ZBB35 glass sample

variation in the mass densities of the glasses as LAC is more sensitive to changes in density compared with MAC. The effect of the Bi_2O_3 content of the glasses is also reflected in their LAC values.

Figure 3 shows the mean free path (MFP) of the glasses estimated from LAC values using Eq. 4 as a function of photon energy. The average distance travelled by a photon with a particular kinetic energy before collision with the particles of an absorbing medium is known as MFP. Figure 3 shows that MFP increased with photon energy up to 6 MeV for ZBB25 and 5 MeV for the other 5 glass samples. Beyond these energies' MFP decreased gradually. The initial increase in the MFP of the glasses with energy is an indication that higher energy photons interact less and thus possess higher MFP. While the gradual decrease in MFP at energies beyond 6 MeV is attributed to the decrease in LAC in this energy region. Among the glasses, the increasing trend of the MFP is the inverse of that of LAC as expected in Eq. 4. Hence, $(ZBB25)_{MFP} > (ZBB30)_{MFP} > (ZBB35)_{MFP} > (ZBB40)_{MFP} > (ZBB45)_{MFP} > (ZBB50)_{MFP}$.

Figure 4(a) shows the variation of HVL with photon energy for all the glasses under study. The HVL is the thickness of a photon attenuating medium that gives $2X = X_o$ (Eq. 1). It is an easy parameter to use when a quick choice of photon shielding material is required. The figure shows that HVL increased with photon energy. This shows that higher glass thickness is required to absorb

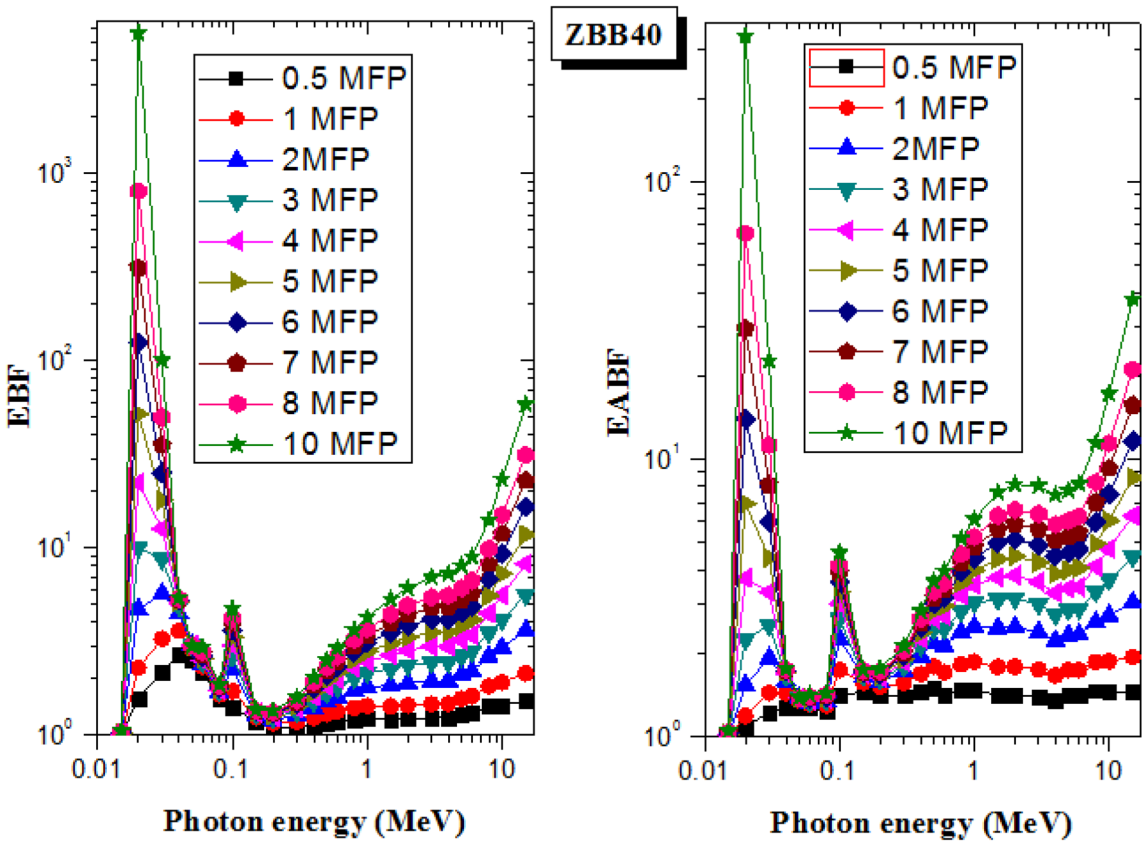

Fig. 9 EBF and EABF as functions of photon energy for ZBB40 glass sample

higher energy photons for the understudied glasses. Also, at higher photon energies, incoherent scattering and pair production interaction processes produce secondary photons. These secondary photons thus require additional material thickness to absorb them. Like the MFP, the HVL of the glasses follow the order $(ZBB25)_{HVL} > (ZBB30)_{HVL} > (ZBB35)_{HVL} > (ZBB40)_{HVL} > (ZBB45)_{HVL} > (ZBB50)_{HVL}$. At 15 MeV, the HVL of the glasses were 1.65, 1.55, 1.47, 1.35, 1.28, and 1.25 cm respectively for ZBB25, ZBB30, ZBB35, ZBB40, ZBB45, and ZBB50. Obviously, the increase in the concentration of Bi_2O_3 caused a reduction in the HVT of the ZBB-glass. HVL of the ZBB-glasses were compared with those of commercial shielding glasses (RS360 and RS520) at photon energies of 200 and 662 keV in Fig. 4b. The figure showed that HVL, ZBB40–50 have lower HVL compared with RS360 and RS520 at the two photon energies. This result implies that ZBB40-50 are better photon shielding glasses compared with RS360 and RS520 and they can thus replace them as choice photon shields for nuclear technological applications.

3.1.2 Z_{eff} and N_{eff} of ZBB-Glasses

The effective atomic number (Z_{eff}) for photons in a medium can be used to assess the interaction between photons and the medium. It is a number that gives the chemical description of composite material the way the atomic number of

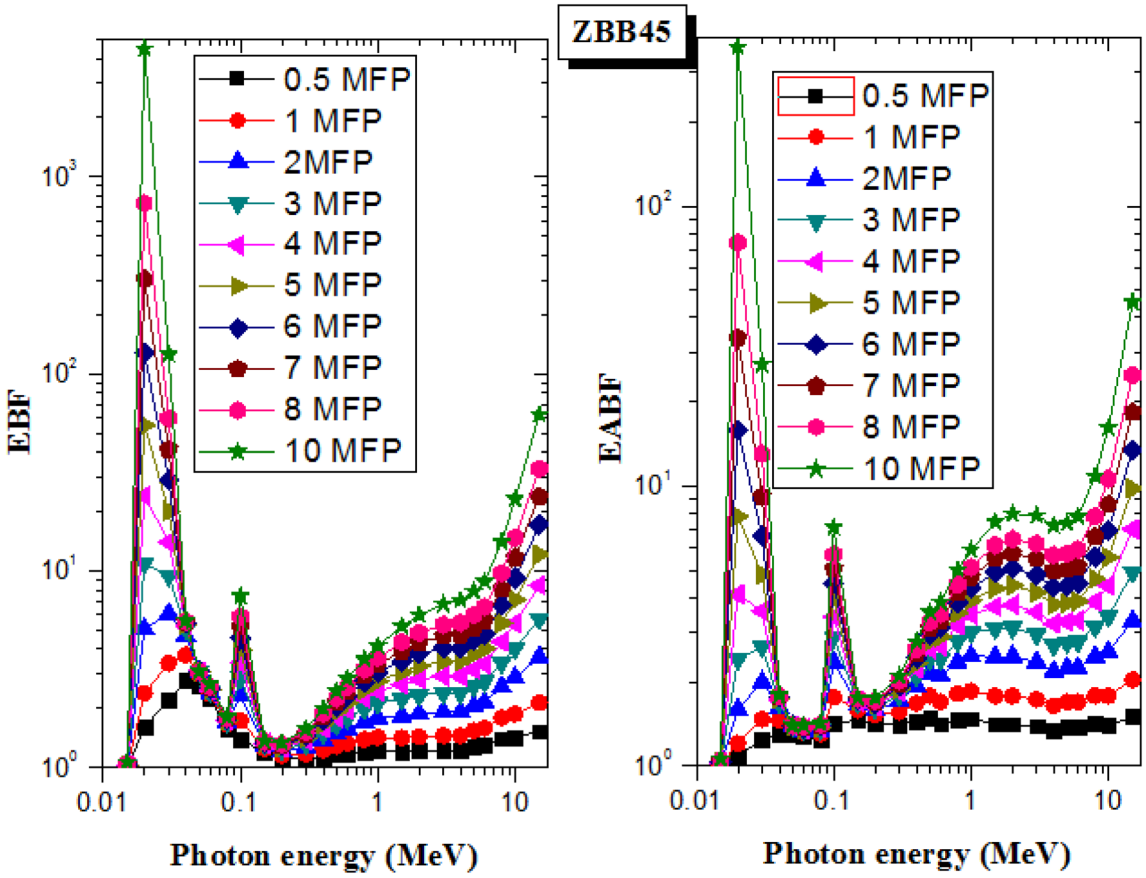

Fig. 10 EBF and EABF as functions of photon energy for ZBB45 glass sample

an element does. However, unlike the atomic number, it is not a constant but varies with photon energy [29]. It can be used to compare photon interaction in diverse media. Values of Z_{eff} of ZBB-glasses with energy are presented in Fig. 5. Throughout the energy spectrum, Z_{eff} changed from: 18.04–47.4, 20.16–49.51, 22.27–51.95, 24.36–53.65, 26.45–55.19 and 28.58–56.61 for ZBB25, ZBB30, ZBB35, ZBB40, ZBB45, and ZBB50, respectively. The range and value of Z_{eff} at each energy is dictated by the chemical components and their proportion in the glass, and photon partial interaction processes [29]. Obviously, the trend of the effective atomic number directly follows the MAC. This is an indication that higher Z_{eff} corresponds to higher photon absorption for different materials. Furthermore, an increase in Bi_2O_3 content increased the effective atomic number of ZBB-glasses. This further showed the inclusion of high atomic number components in any glass matrix will ultimately increase the effective atomic number of such glasses.

Figures 6, 7, 8, 9, 10 and 11 show the change of EABF and EBF as functions of photon energy for penetration depths up to 10 MFP in ZBB-glasses. The variations in

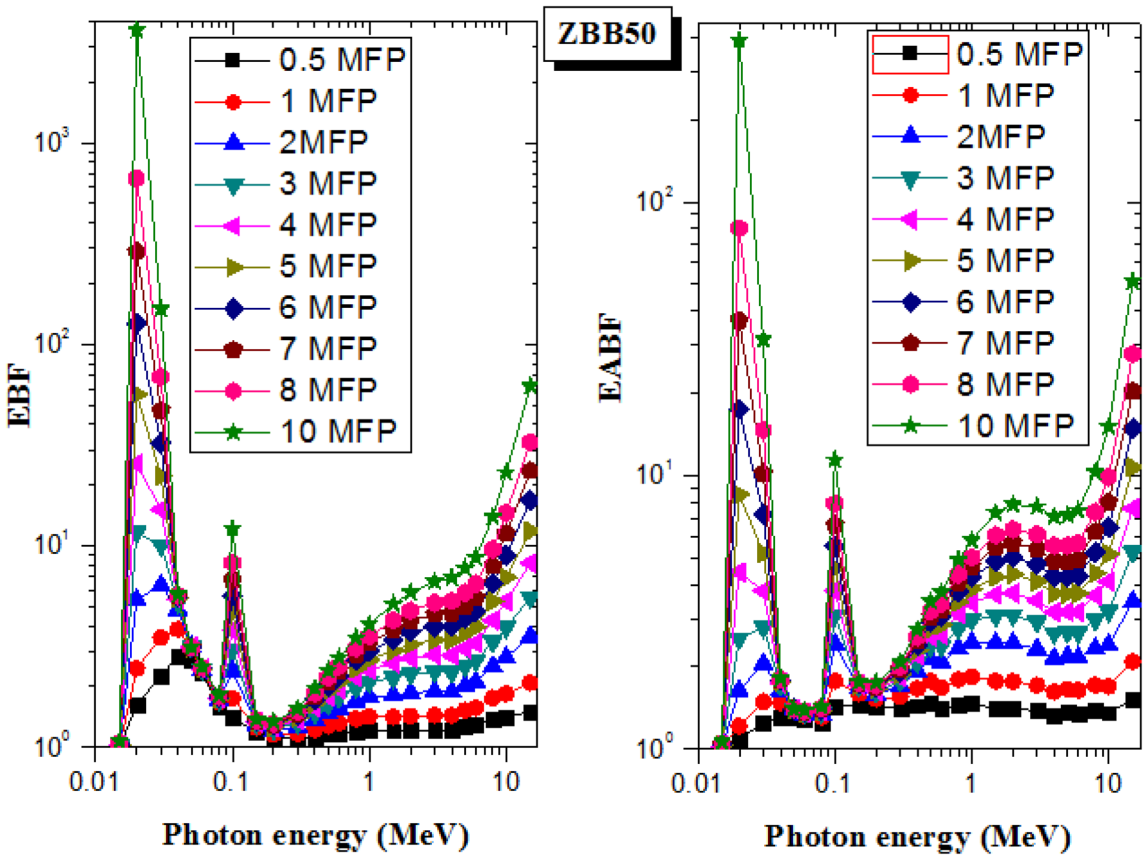

Fig. 11 EBF and EABF as functions of photon energy for ZBB50 glass sample

the values of the buildup factors with respect to photon energy looks similar for all the glasses. The buildup factors enhanced with energy at each depth with peaks at 0.02 and 0.1 MeV due to Bi absorption edges. The low EABF and EBF at lower energies are due to the contribution of the photoelectric absorption process which removes photons and hence prevents buildup. Compton scattering process is responsible for high buildup of photons at energies beyond the photoelectric interaction dominated range. At depths beyond 5 MFP, the buildup factor continues to grow with energy up to maximum photon energy of 15 MeV with a slight trough at 6 MeV. This is so as scattered photons and those produced via the pair production interactions interact to produce more secondary photons (buildup). Such increase in buildup factors is observed in materials including high atomic number composite like Mo, Pb, Bi etc. [27, 42, 43]. EABF and EBF of the ZBB-glasses are compared as shown in Figs. 12, 13, 14 and 15 for energies of 0.015, 0.15, 1.5 and 15 MeV showed that both buildup factors increased with penetration depth. Also, EABF and EBF increase with Bi_2O_3 content of the glasses except at 1.5 MeV where the reverse was the case. The implies that the buildup factors in the glasses increase depending on their effective atomic number. However, at 1.5 MeV where Compton interaction cross section dominates which is independent of the atomic number but electron density. It is thus evident that the number of electrons per unit mass is highest in ZBB25 and least in

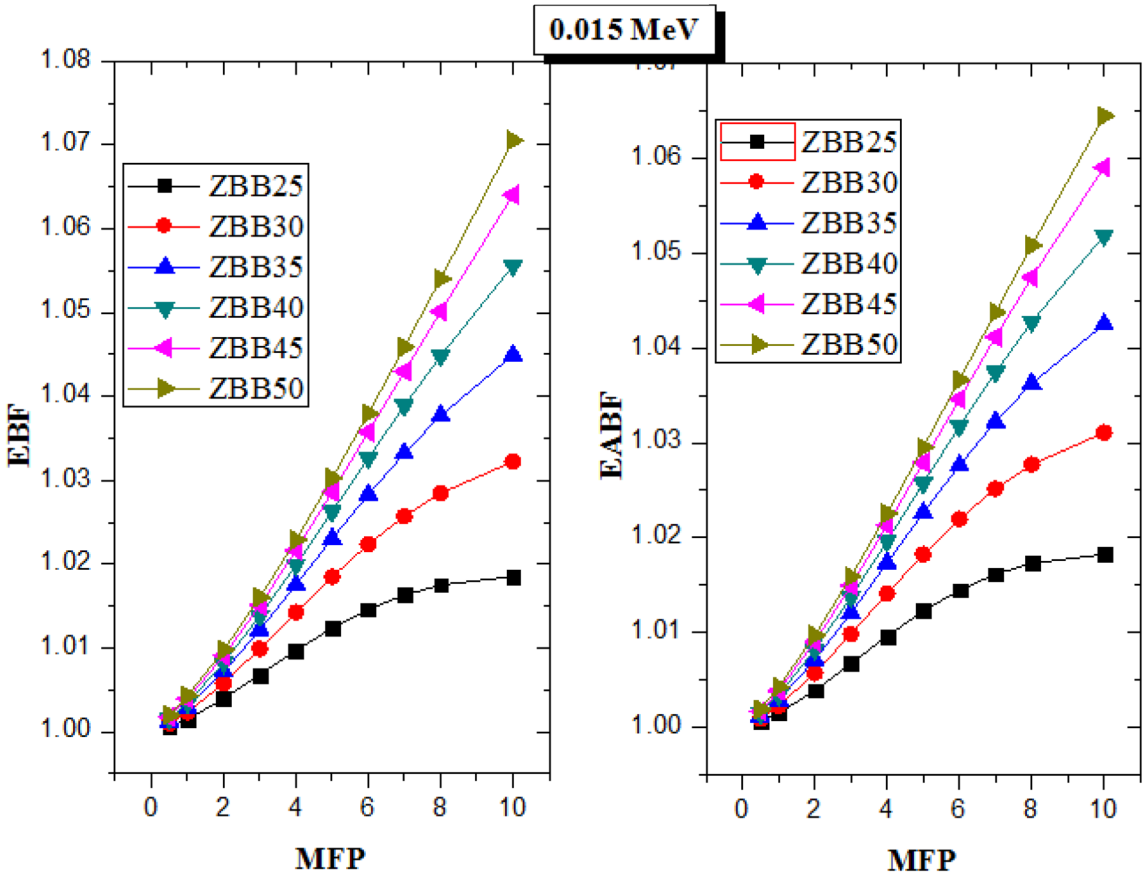

Fig. 12 Variation of *EABF* and *EBF* with penetration depth at 0.015 MeV for ZBB-glasses

ZBB50. Thus, ZBB25 presents the highest buildup factors among the glasses at this energy.

Figure 16 shows the effective LAC (ELAC) as calculated from Eq. 8 as a function of depth and for 4 selected energies (0.015, 0.15, 1.5, and 15 MeV). The result showed that at least energy, ELAC has no noticeable change with respect to depth, however, beyond this energy as the depth increased, ELAC also improved as expected. It therefore means that with thicker absorber, absorption is higher. Comparing the effective LAC of the glasses, ZBB50 possesses the greatest absorption coefficient for all the considered energy and depth. The effect of the inclusion and increase in Bi_2O_3 content of ZBB-glasses is to improve their photon shielding capacity.

3.1.3 Σ_R and Σ_T of ZBB-Glasses

Table 2 presents the calculated values of partial densities and macroscopic fast neutron removal cross section, Σ_R of ZBB25—ZBB50 glasses. The result showed that there was

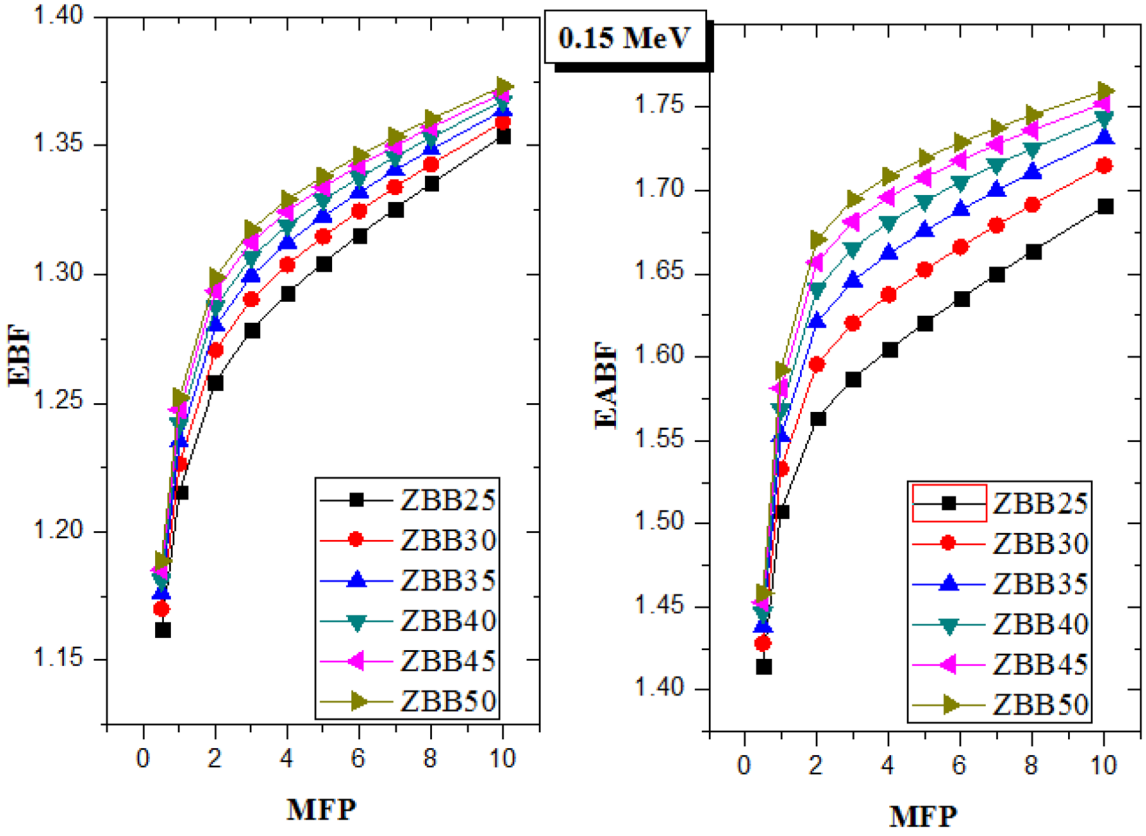

Fig. 13 Variation of *EABF* and *EBF* with penetration depth at 0.15 MeV for ZBB-glasses

13, 24, 38, 50 and 57% increase in the values of Σ_R for ZBB30, ZBB35, ZBB40, ZBB45, and ZBB50 respectively with respect to that of ZBB25. The increase in the partial density of Bi due to the increase in the Bi_2O_3 content of ZBB-glasses lead to a corresponding higher fast neutron removal cross section. Hence ZBB50 had the highest Σ_R among the ZBB glasses. Comparing the value of Σ_R for ZBB25- 50 with those of water (0.1024 cm^{-1}), ordinary concrete (OC) (0.094 cm^{-1}) and recently developed glass system- TVM60 (0.1055 cm^{-1}) [42], it is obvious that the ZBB-glasses are poor fast neutron absorber compared to these media. This is due to the high concentration of heavy elements such as Bi which are not good absorbers of fast neutrons in the glass composition.

Furthermore, the calculated total thermal neutron cross-sections of the ZBB-glasses are given in Table 3. The table showed that Σ_T reduced from 15.45 to 7.62 cm^{-1} for the ZBB-glasses as the Bi_2O_3 content increased from 25 to 50 mol%. This represents a 51% reduction between Σ_T of ZBB25 and ZBB50. This reduction is directly due to the reduction of B in the glasses as Bi_2O_3 content increased. since B is a good thermal neutron absorber, reducing the B_2O_3 content of the glass correspondingly led to the reduction of thermal neutron absorption capacity of the glass. Comparing the Σ_T of ZBB-glasses with those of recently

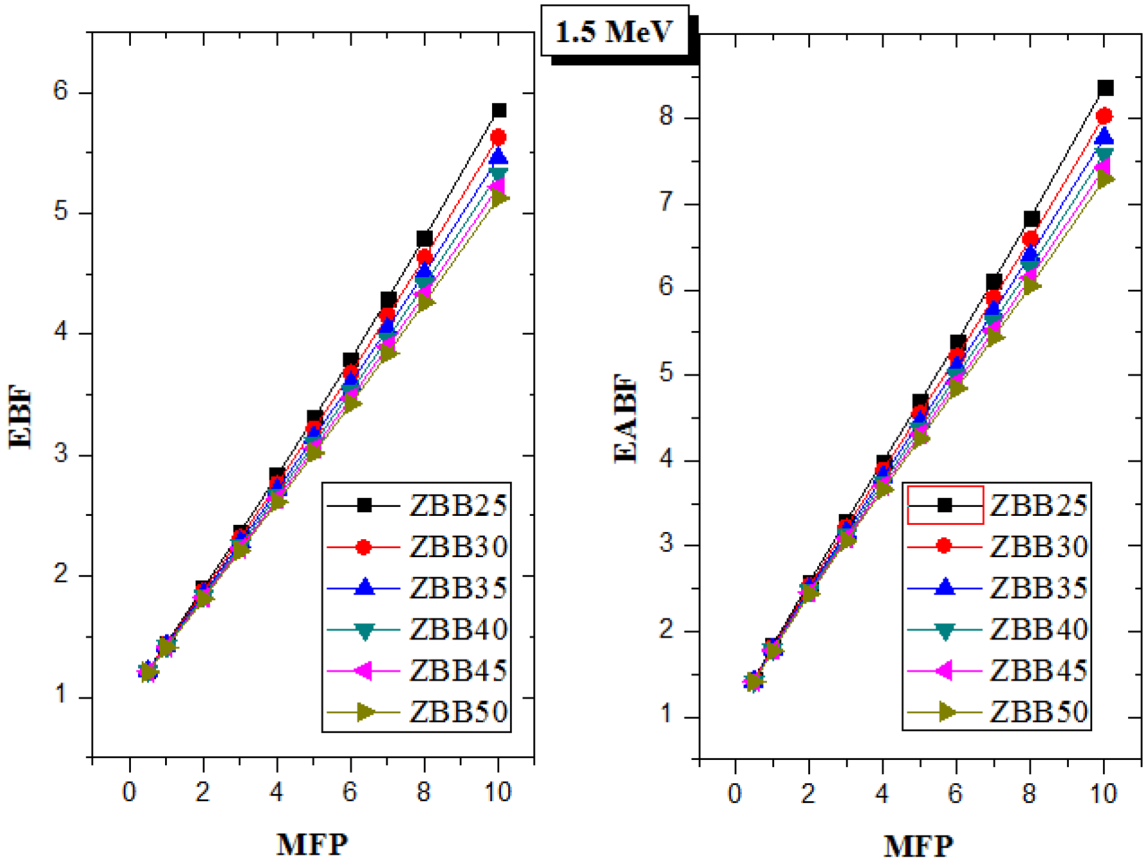

Fig. 14 Variation of *EABF* and *EBF* with penetration depth at 1.5 MeV for ZBB-glasses

published bismuth boro-tellurite glass systems [44], it is obvious that the ZBB-glasses are better thermal neutron absorber with ZBB25 being the best.

3.1.4 TMSP and Projected Range (R) of Proton and Alpha Particle for ZBB-Glasses

The changes in the total MSP (TMSP) of alpha (α)-particle and proton in ZBB- glasses are illustrated in Fig. 17. The changes for both proton and α are similar for all the glasses; increasing with energy until a maximum value is reached then sliding down as energy grows. The highest TMSP was obtained at energy of 0.09 MeV and 1 MeV for *p* and α-particle respectively in all the investigated glasses. This is because of low energy loss of alpha particle per interaction thus the maximum (peak) TMSP is delayed for alpha particles compared to protons for the same energy spectra in similar material. It was also observed that TMSP for **α-**particle

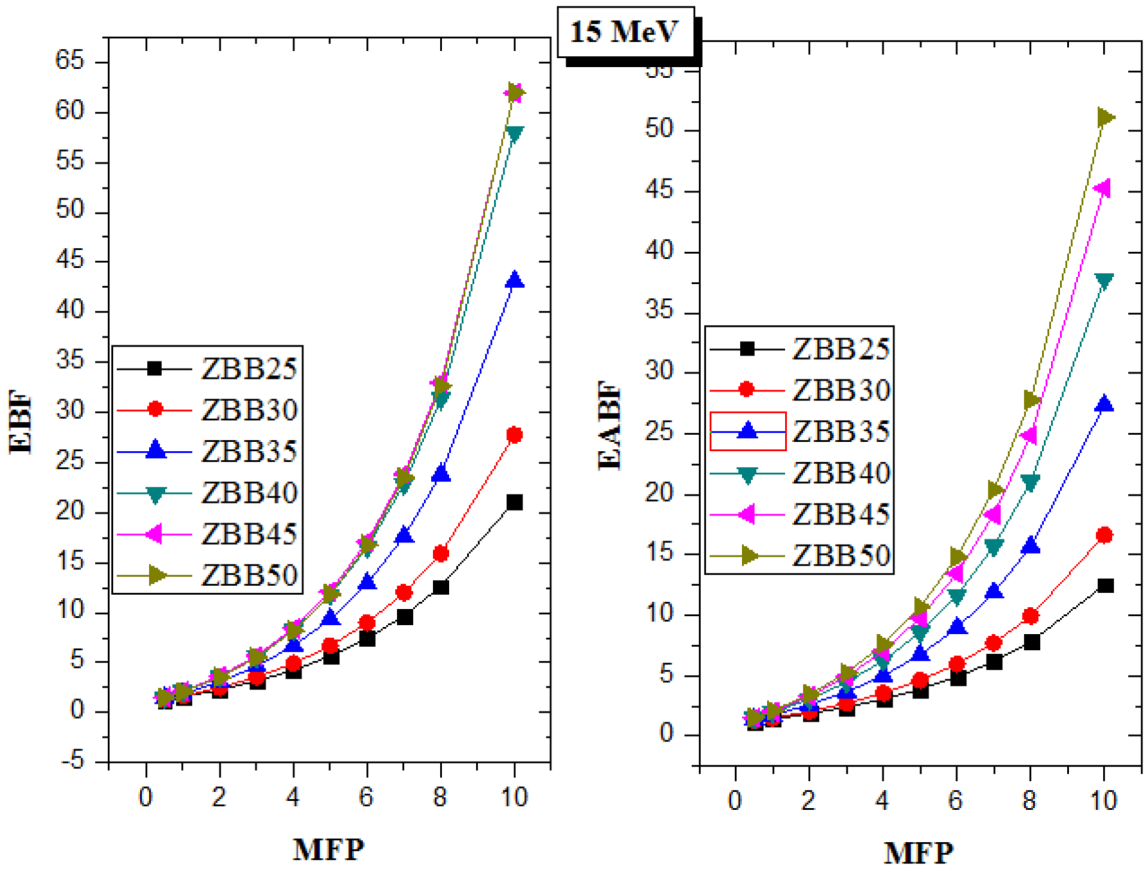

Fig. 15 Variation of *EABF* and *EBF* with penetration depth at 15 MeV for ZBB-glasses

was higher than that of p. This is because of a higher electrical charge and lower velocity of alpha compared to those of p. TMSP is directly proportional to ion charge and inversely proportional to the square of its velocity. At equal kinetic energy, **α-**particle have lower velocity than p coupled with its higher charge, thus higher TMSP. According to Fig. 17, the trend in TMSP follows the order: $(ZBB25)_{TMSP} > (ZBB30)_{TMSP} > (ZBB35)_{TMSP} > (ZBB40)_{TMSP} > (ZBB45)_{TMSP} > (ZBB50)_{TMSP}$ for both p and alpha particles.

The values of projected range (R) of p and α in the ZBB-glasses as a function of kinetic energy of projectile ions is illustrated in Fig. 18. Generally, the projected range increased in all the glasses as the particle's kinetic energy increased; an indication that more energetic ion is more penetrating. The values of the projected range are very close; however, the trend of the calculated projected range follows the order: $(ZBB25)_R < (ZBB30)_R < (ZBB35)_R < (ZBB40)_R < (ZBB45)_R < (ZBB50)_R$ for both p and alpha particle. Thus, ZBB50 is a better proton and alpha particle absorber compared to the other ZBB-glasses considered herein.

3.2 Elastic Moduli of ZBB-Glasses

As shown in Fig. 19 and Table 4, the values of ($K_{B\text{-}C}$) were found to decrease from 81.58 to 66.55 GPa. This decrease can be interpreted based on the dependence of the ($K_{B\text{-}C}$) on the number of the network bonds per unit volume (n_b) and the average bond lengths (l), which is related to the first-order stretching-force constant [40]. The addition of Bi_2O_3

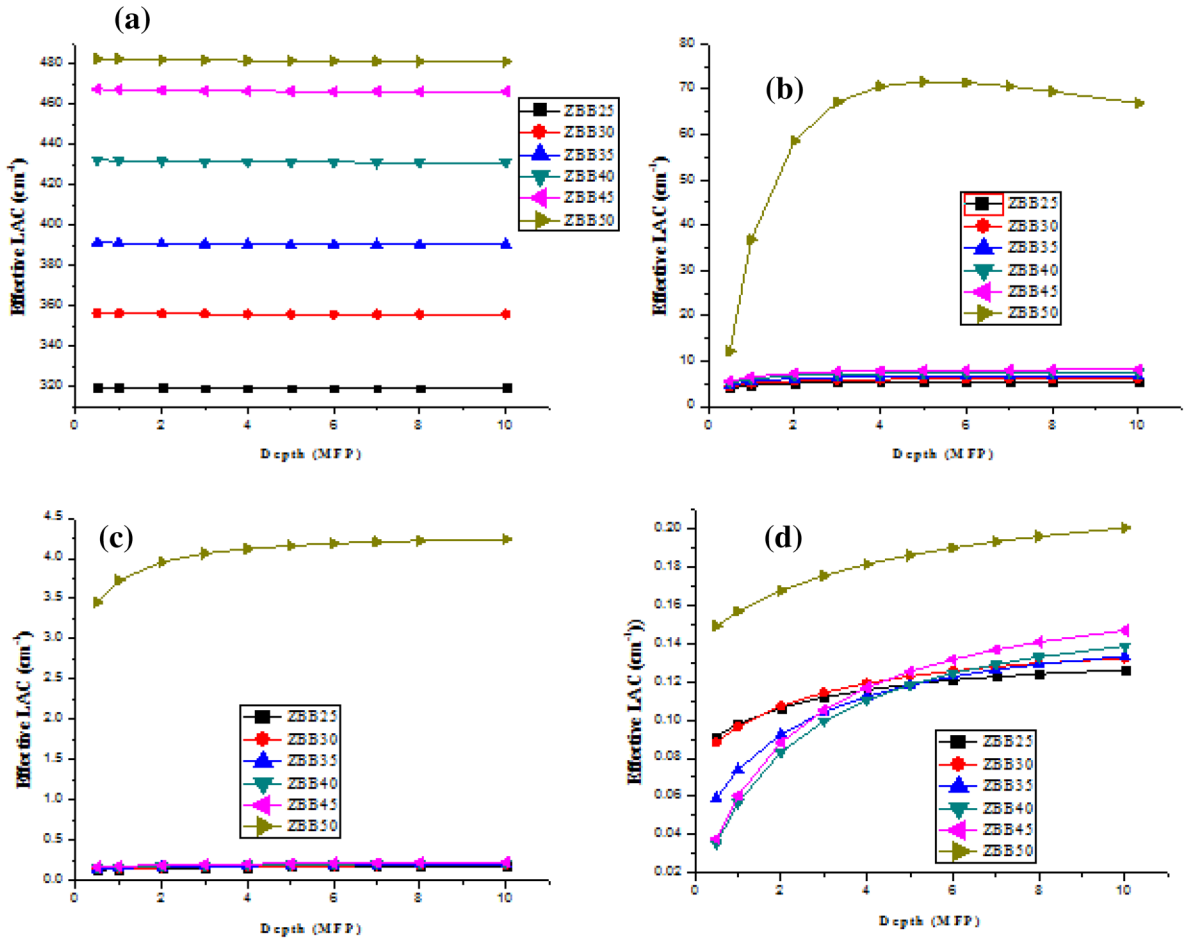

Fig. 16 Variation of effective LAC with penetration depth **(a)** 0.015 **(b)** 0.15 **(c)** 1.5, and **(d)** 15 MeV for ZBB-glasses

Table 2 Partial density and macroscopic removal cross section of ZBB-glasses

Glass code	Density (g/cm^3)	Partial density (g/cm^3)				Σ_R(cm^{-1})				Total Σ_R(cm^{-1})
		Bi	Zn	O	B	Bi	Zn	O	B	
ZBB25	4.265	2.6234	0.1642	1.1242	0.3531	0.027	0.003	0.0455	0.0203	0.027
ZBB30	4.468	2.9534	0.1541	1.0548	0.3055	0.0304	0.0028	0.0427	0.0175	0.0304
ZBB35	4.675	3.264	0.1458	0.9995	0.2655	0.0336	0.0026	0.0404	0.0152	0.0336
ZBB40	4.972	3.6245	0.1417	0.971	0.2346	0.0373	0.0025	0.0393	0.0134	0.0373
ZBB45	5.213	3.9347	0.1371	0.9372	0.2038	0.0405	0.0025	0.0379	0.0117	0.0405
ZBB50	5.313	4.1282	0.1291	0.8846	0.171	0.0425	0.0023	0.0358	0.0098	0.0425

Table 3 Total thermal neutron cross-sections (Σ_T) of ZBB-glasses

Glass code	Density (g/cm^3)	σ_T (cm^{-1})				Total Σ_T (cm^{-1})
		Bi	Zn	O	B	
ZBB25	4.265	0.0694	0.0079	0.1791	15.1945	15.4509
ZBB30	4.468	0.0782	0.0074	0.168	13.1475	13.4011
ZBB35	4.675	0.0864	0.007	0.1592	11.4253	11.6779
ZBB40	4.972	0.096	0.0068	0.1547	10.0974	10.3549
ZBB45	5.213	0.1042	0.0066	0.1493	8.7700	9.0301
ZBB50	5.313	0.1093	0.0062	0.1409	7.3609	7.6173

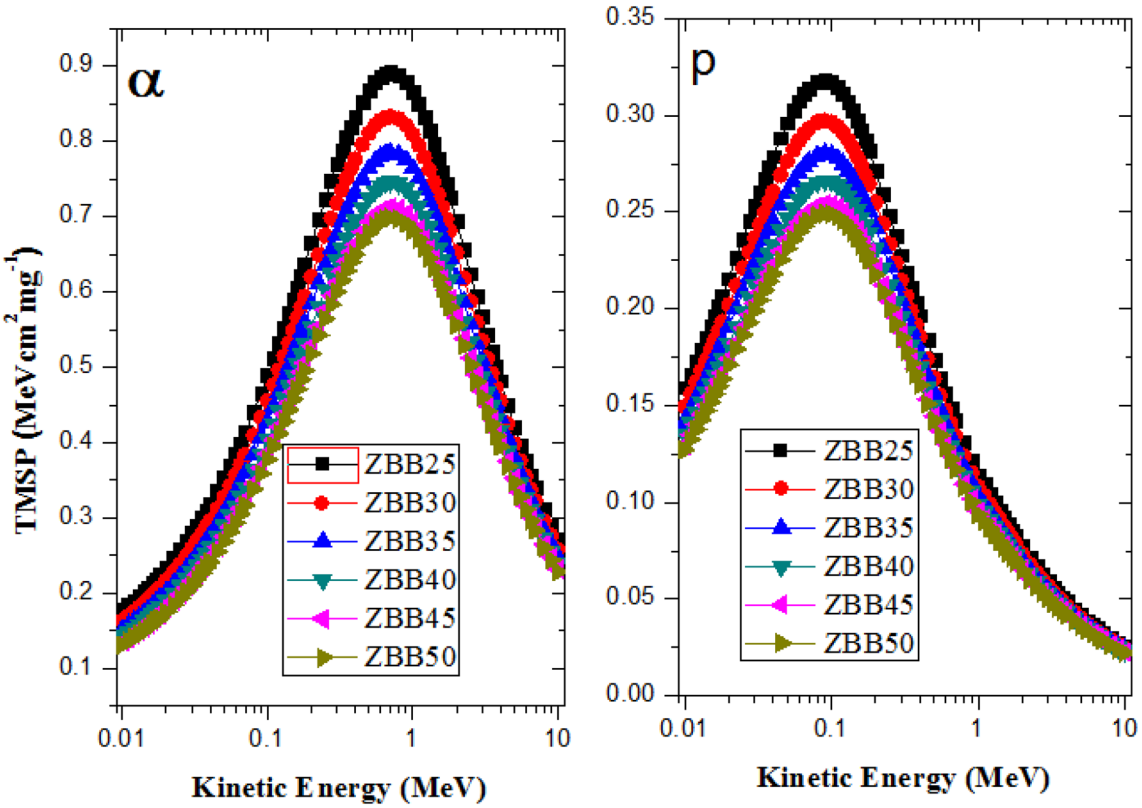

Fig. 17 Variation of TMSP for alpha and proton particles as a function of kinetic energy

causes (n_b) to decrease from 4.98 to 3.92 [$\times 10^{28}$ (m^{-3})] despite of the decreases in the average stretching-force constant ($\overline{F}$) from 478.9 to 378 (N/m). Also, the average crosslink density is constant due to the same coordination number of B_2O_3 and Bi_2O_3. Theoretically, the estimated values of the calculated bond compression elastic moduli [shear ($S_{B\text{-}C}$), longitudinal ($L_{B\text{-}C}$), and Young's ($E_{B\text{-}C}$)] were found to decrease from 35.95 to 29.33 GPa, from 129.40 to 105.57 GPa and from 94.05 to 76.73 GPa, respectively. Values of theoretical Poisson's ratio ($\sigma_{B\text{-}C}$) were constant due to the same coordination number of B_2O_3 and Bi_2O_3.

The second theoretical treatment for calculating the moduli of elasticity of ZBB-glasses is based on the Makishima and Mackenzi model [40–42]. For this model, coordination number per cation (n_f), crosslink density per cation (n_c), Stretching force constant (F), packing density factor (V_i), and dissociation/bond energy per unit volume (G_i) of ZnO, B_2O_3, and Bi_2O_3 oxides are collected and tabulated in Table 5. Tables 6 gives the values of the total packing density (V_t), total dissociation energy (G_t), Young's modulus ($E_{M\text{-}M}$), bulk modulus ($K_{M\text{-}M}$), shear modulus ($S_{M\text{-}M}$), and Poisson's ratio ($\sigma_{M\text{-}M}$) based on Makishima-Mackenzie model of ZBB-glasses. It is clear that, the decreasing in the

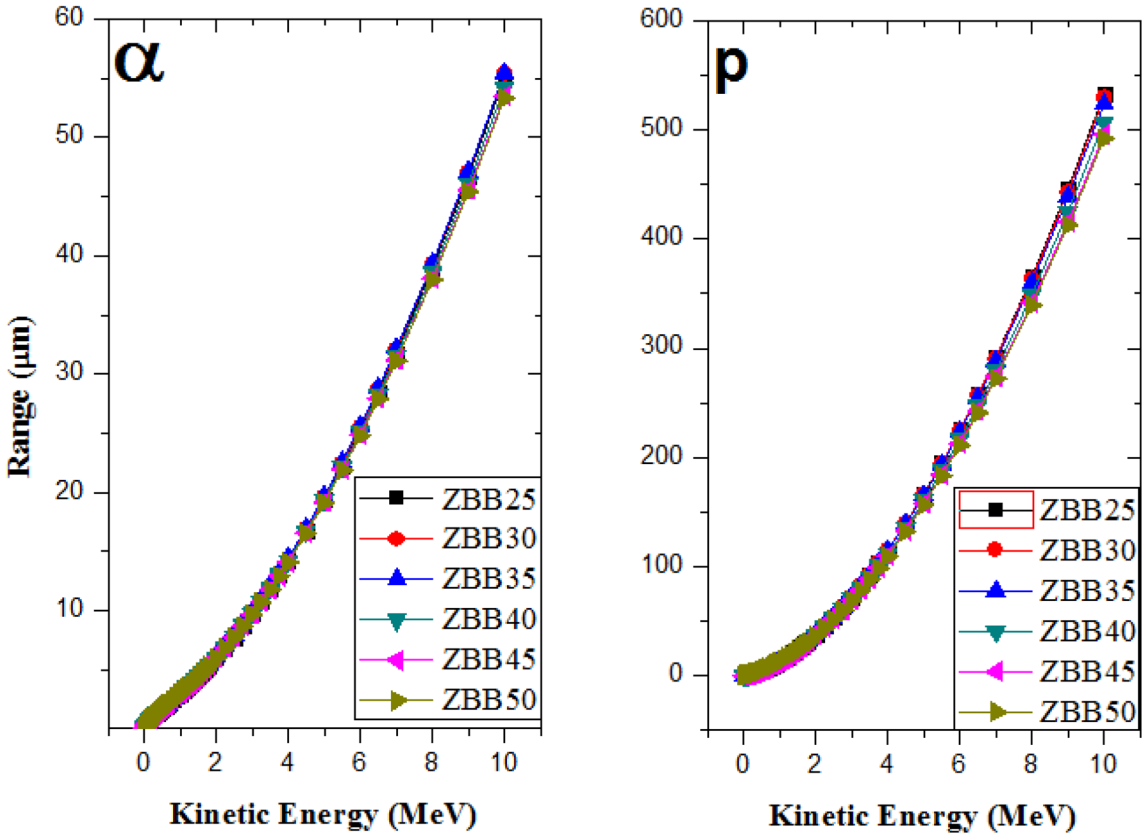

Fig. 18 Variation of the range of alpha and proton particles as a function of kinetic energy

total packing density of the glass from 0.43 to 0.39 which is attributed to the higher value of ionic radius of B_2O_3 than Bi_2O_3.The increasing the Bi_2O_3 leads to increase the total dissociation energy per unit volume of the system from 27.58 to 29.83 kJ/cm^3. This is due to the substitution of Bi_2O_3 which have dissociation energy (31.6 $\frac{kj}{cm^3}$) by B_2O_3 which have dissociation energy (22.6 $\frac{kj}{cm^3}$). The Calculated values of ($E_{M\text{-}M}$), ($K_{M\text{-}M}$), and ($S_{M\text{-}M}$) elastic moduli based on Makishima -Mackenzie model were increased as values in Table 6 and Fig. 20. Values of Poisson's ratio ($\sigma_{M\text{-}M}$) were 0.178, 0.167, 0.160, 0.159, 0.157, and 0.147 for ZBB25, ZBB30, ZBB35, ZBB40, ZBB45, and ZBB50 glasses, respectively.

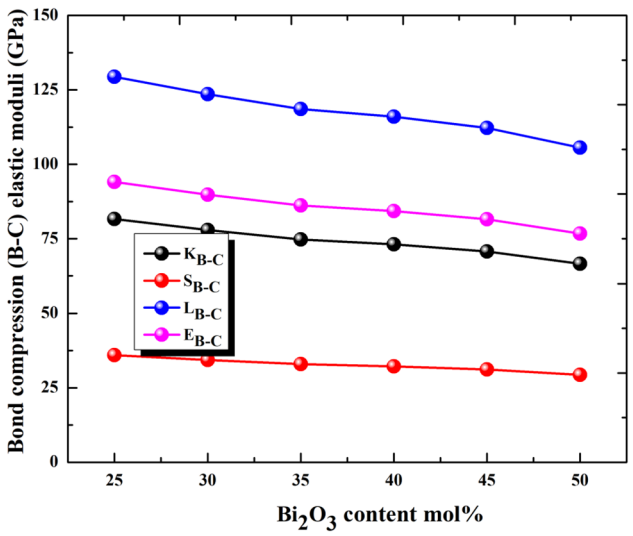

Fig. 19 Elastic moduli via bond compression (B-C) model of 10ZnO-(90-x)B_2O_3-xBi_2O_3:(ZBB): x = 25–50 mol% glasses

4 Conclusion

The main objective of the current work is to investigate the role of Bi_2O_3 content in photon, alpha particle, proton, fast and thermal neutron shielding capacity and elastic moduli of 10ZnO-(90-x)B_2O_3-xBi_2O_3 (ZBB-glasses): x = 25–50 mol%. The values of mass attenuation coefficient in the ZBB-glasses were mostly influenced by the mass density and Bi-content of the glasses. The MAC, LAC values of the glasses improved with increase in Bi_2O_3 molar concentrations in ZBB-glasses. All the photon absorbing parameters indicated that photon shielding

Table 4 The values of total number of cationic per glass formula unit (η), average cross-link density ($\overline{n}_c$), average stretching force constant ($\overline{F}$), number of network bond per unit volume (n_b), average bond length (l), calculated bond compression elastic moduli (bulk ($K_{B\text{-}C}$), shear ($S_{B\text{-}C}$), longitudinal ($L_{B\text{-}C}$), Young's ($E_{B\text{-}C}$)) and Poisson's ratio ($\sigma_{B\text{-}C}$) of ZBB-glasses

Parameters and elastic moduli	ZBB25	ZBB30	ZBB35	ZBB40	ZBB45	ZBB50
η	1.9	1.9	1.9	1.9	1.9	1.9
$\overline{n}_c = \frac{1}{\eta}\sum x_i(n_c)_i(N_C)_i$	0.684	0.684	0.684	0.684	0.684	0.684
$\overline{F} = \frac{\sum(xn_f f)_i}{\sum(xn_f)_i}(N/m)$	478.909	458.727	438.545	418.363	398.181	378
$n_b = \frac{N_A}{V_m}\sum(n_f x)_i \times 10^{28}\,(m^{-3})$	4.989	4.680	4.434	4.308	4.158	3.925
$l = \left(0.0106\frac{\overline{F}}{K_{B-C}}\right)^{0.26}(nm)$	0.485	0.486	0.485	0.482	0.480	0.481
$K_{B-C} = \frac{N_A}{9V_m}\sum_i(n_f x\overline{F}r^2)_{(GPa)}$	81.586	77.914	74.731	73.130	70.718	66.559
$S_{B-C} = \left(\frac{3}{2}\right)K_{B-C}\left(\frac{1-2\sigma_{B-C}}{1+\sigma_{B-C}}\right)$(GPa)	35.956	34.338	32.935	32.230	31.167	29.334
$L_{B-C} = K_{B-C} + \frac{4}{3}S_{B-C}(GPa)$	129.409	123.585	118.536	115.997	112.171	105.574
$E_{B-C} = 2S_{B-C}(1+\sigma_{B-C})(GPa)$	94.053	89.821	86.151	84.306	81.525	76.730
$\sigma_{B-C} = 0.28(\overline{n}_c)^{-0.25}$	0.307	0.307	0.307	0.307	0.307	0.307

Table 5 Coordination number per cation (n_f), crosslink density per cation (n_c), Stretching force constant (F), packing density factor (V_i), and dissociation/bond energy per unit volume (G_i) of the oxides ZnO—B_2O_3—Bi_2O_3

Oxide	n_f	n_c	F (N/m)	V_i (m^3/mol)	$G_i \times 10^6$ (KJ/m^3)
ZnO	6	4	219	7.9	49.9
B_2O_3	3	1	660	15.2	22.6
Bi_2O_3	3	1	216	26.1	31.6

increased with mass density and Bi_2O_3 content. All the ZBB-glasses showed almost similar charged particle shielding capacity. However, ZBB50 had a comparable charged particle absorption efficiency. There was a 57% growth in fast neutron removal cross section as Bi_2O_3 molar concentration increased to 50% in the ZBB-glass matrix. ZBB50 possesses the highest fast neutron removal cross section among the ZBB-glasses. In terms of thermal neutron absorbing capacity, the presence of B in the glass matrix ensures that the ZBB-glasses are good thermal neutron absorption. ZBB25 has the highest thermal neutron absorption capacity among the investigated glasses. Generally, ZBB-glasses can be adopted for photon, thermal neutron, proton, and alpha particle shielding purposes. In addition, elastic (shear, longitudinal, and Young's) moduli and Poisson's ratio are changed significantly with the increase of Bi_2O_3 content mol% in ZBB-glasses.

Table 6 Total ionic packing density (V_t), total dissociation energy (G_t), Young's modulus ($E_{M\text{-}M}$), bulk modulus ($K_{M\text{-}M}$), shear modulus ($S_{M\text{-}M}$), and Poisson's ratio ($\sigma_{M\text{-}M}$) based on Makishima-Mackenzie model of ZBB-glasses

Parameters and elastic moduli	ZBB25	ZBB30	ZBB35	ZBB40	ZBB45	ZBB50
$V_t = \left(\frac{1}{V_m}\right)\sum_i(V_i x_i)$	0.431701	0.417841	0.408008	0.408248	0.405395	0.393496
$G_t = \sum_i(G_i x_i)(KJ/m^3)$	27.58	28.03	28.48	28.93	29.38	29.83
$E_{M-M} = 2V_t G_t(GPa)$	23.812	23.424	23.240	23.621	23.821	23.475
$K_{M-M} = 1.2V_t E_{M-M}(GPa)$	12.335	11.745	11.378	11.572	11.588	11.085
$S_{M-M} = (3E_{M-M}K_{M-M})/(9K_{M-M} - E_{M-M})$ (Gpa)	10.104	10.030	10.020	10.183	10.290	10.233
$\sigma_{M-M} = \left(\frac{E_{M-M}}{2G_{M-M}}\right) - 1_{(GPa)}$	0.178	0.167	0.160	0.159	0.157	0.147

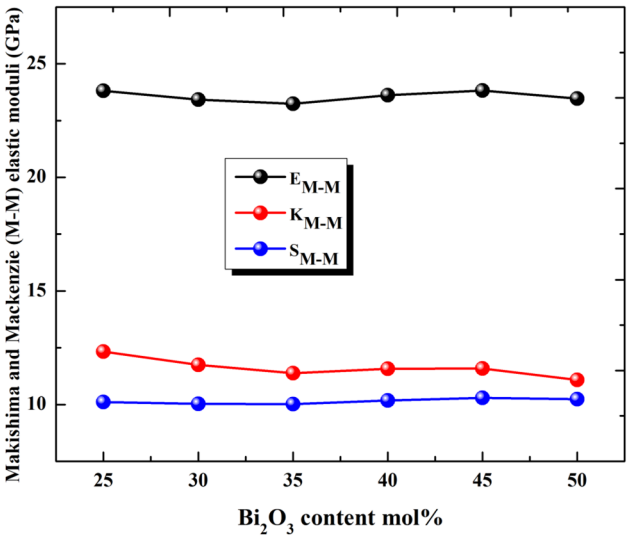

Fig. 20 Elastic moduli via Makishima-Mackenzie (M-M) model of ZBB-glasses

Acknowledgements Taif University Researchers Supporting Project number (TURSP-2020/84), Taif University, Taif, Saudi Arabia.

References

1. K. Kaur, K.J. Singh, V. Anand, Correlation of gamma ray shielding and structural properties of PbO-BaO-P_2O_5 glass system. Nucl. Eng. Des. **285**, 31–38 (2015). https://doi.org/10.1016/j.nucengdes.2014.12.033
2. O. Olarinoye, C. Oche, Gamma-rays and fast neutrons shielding parameters of two new Ti-based bulk metallic glasses, Iranian Journal of Medical Physics (2020)
3. M.I. Sayyed, I.A. El-Mesady, A.S. Abouhaswa, A. Askin, Y.S. Rammah, Comprehensive study on the structural, optical, physical and gamma photon shielding features of B_2O_3-Bi_2O_3-PbO-TiO_2 glasses using WinXCOM and Geant4 code. J. Mol. Struct. **1197**, 656–665 (2019)
4. M.S. Al-Buriahi, F.I. El-Agawany, C. Sriwunkum, H. Akyıldırım, H. Arslan, B.T. Tonguc, Y.S. Rammah, Influence of Bi_2O_3/PbO on nuclear shielding characteristics of lead-zinc-tellurite glasses. Phys. B **581**, 411946 (2020)
5. M.S. Al-Buriahi, Y.S. Rammah, Investigation of the physical properties and gamma-ray shielding capability of borate glasses containing PbO, Al_2O_3 and Na_2O. Appl. Phys. A **125**, 717 (2019)
6. Y.S. Rammah, M.S. Al-Buriahi, A.S. Abouhaswa, B_2O_3–$BaCO_3$–Li_2O_3 glass system doped with Co_3O4: Structure, optical, and radiation shielding properties. Phys. B **576**, 411717 (2020)
7. D.K. Gaikwad, S.S. Obaid, M.I. Sayyed, R.R. Bhosale, V.V. Awasarmol, A. Kumar, M.D. Shirsat, P.P. Pawar, Comparative study of gamma ray shielding competence of WO_3-TeO2-PbO glass system to different glasses and concretes. Mater Chem. Phys. **213**, 508–517 (2018)
8. C. Bootjomchai, J. Laopaiboon, C. Yenchai, R. Laopaiboon, Gamma-ray shielding and structural properties of barium-bismuth-borosilicate glasses. Radiat. Phys. Chem. **81**, 785–790 (2012). https://doi.org/10.1016/j.radphyschem.2012.01.049
9. A.A.A. Darwish, S.A.M. Issa, M.M. El-Nahass, Effect of gamma irradiation on structural, electrical, and optical properties of nanostructure thin films of nickel phthalocyanine. Synth. Methods **215**, 200–206 (2016). https://doi.org/10.1016/j.synthmet.2016.03.002
10. B.O. Elbashir, M.G. Dong, M.I. Sayyed, S.A.M. Issa, K.A. Matori, M.H.M. Zaid, Comparison of Monte Carlo simulation of gamma-ray attenuation coefficients of amino acids with XCOM program and experimental data. Results Phys. **9**, 6–11 (2018). https://doi.org/10.1016/j.rinp.2018.01.075
11. V. Beir, Health Effects of Exposure to Low Levels of Ionizing Radiation, 1990
12. S. Issa, M. Sayyed, M. Kurudirek, Investigation of gamma radiation shielding properties of some zinc tellurite glasses. J. Phys. Sci. **27**, 97–119 (2016). https://doi.org/10.21315/jps2016.27.3.7
13. S.A.M. Issa, A.A.A. Darwish, M.M. El-Nahass, The evolution of gamma-rays sensing properties of pure and doped phthalocyanine. Prog. Nucl. Energy **100**, 276–282 (2017). https://doi.org/10.1016/j.pnucene.2017.06.016
14. S.A.M. Issa, T.A. Hamdalla, A.A.A. Darwish, Effect of $ErCl_3$ in gamma and neutron parameters for different concentration of $ErCl_3$-SiO_2 (EDFA) for the signal protection from nuclear radiation. J. Alloys Compd. **698**, 234–240 (2017)
15. S. Kaewjaeng, J. Kaewkhao, P. Limsuwan, U. Maghanemi, Effect of BaO on optical, physical and radiation shielding properties of SiO_2-B_2O_3-Al_2O_3-CaO-Na_2O glasses system. Procedia Eng. **32**, 1080–1086 (2012). https://doi.org/10.1016/j.proeng.2012.02.058
16. R. Mirji, B. Lobo, Computation of the mass attenuation coefficient of polymeric materials at specific gamma photon energies. Phys. Chem. Radiat. **135**, 32–34 (2017). https://doi.org/10.1016/j.radphyschem.2017.03.001
17. K.J. Singh, S. Kaur, R.S. Kaundal, Comparative study of gamma ray shielding and some properties of PbO–SiO_2–Al_2O_3 and Bi_2O_3–SiO_2–Al_2O_3 glass systems. Radiat. Phys. Chem. **96**, 153–157 (2014). https://doi.org/10.1016/j.radphyschem.2013.09.015
18. Y.S. Rammah, F.I. El-Agawany, K.A. Mahmoud, R. El-Mallawany, Erkan Ilik, Gokhan Kilic, FTIR, UV–Vis–NIR spectroscopy, and gamma rays shielding competence of novel ZnO-doped vanadium borophosphate glasses. J. Mater. Sci.: Mater. Electron. (2020). https://doi.org/10.1007/s10854-020-03440-5
19. A.A. Ali, Y.S. Rammah, M.H. Shaaban, The influence of TiO_2 on structural, physical and optical properties of B_2O_3 –TeO_2 – Na_2O – CaO glasses. J. Non-Cryst. Solids **514**, 52–59 (2019)
20. Y.S. Rammah, G. Kilic, R. El-Mallawany, U. Gökhan Issever, F.I. El-Agawany, Investigation of optical, physical, and gamma-ray shielding features of novel vanadyl boro-phosphate glasses. J. Non-Cryst. Solids **533**, 119905 (2020)
21. Y.S. Rammah, F.I. El-Agawany, K.A. Mahmoud, A. Novatski, R. El-Mallawany, Role of ZnO on TeO_2. Li_2O. ZnO glasses for optical and nuclear radiation shielding applications utilizing MCNP5 simulations and WinXCOM program. J. Non-Cryst. Solids **544**, 120162 (2020)
22. Y.S. Rammah, M.I. Sayyed, A.A. Ali, H.O. Tekin, R. El-Mallawany, Optical properties and gamma shielding features of bismuth borate glasses. Appl. Phys. A **124**, 824–832 (2018)
23. M.I. Sayyed, Bismuth modified shielding properties of zinc boro-tellurite glasses. J. Alloy. Compd. **688**, 111–117 (2016)
24. Y.S. Rammah, I.O. Olarinoye, F.I. El-Agawany, A. El-Adawy, A. Gamal, E.S. Yousef, Elastic moduli, photon, neutron, and proton shielding parameters of tellurite bismo-vanadate (TeO_2–V_2O_5–Bi_2O_3) semiconductor glasses. Ceramics Int. **46**(16), 25440–25452 (2020). https://doi.org/10.1016/j.ceramint.2020.07.014
25. B.O. El-Bashir, M.I. Sayyed, M.H.M. Zaid, K.A. Matori, Comprehensive study on physical, elastic and shielding properties of

ternary BaO-Bi_2O_3-P_2O_5 glasses as a potent radiation shielding material. J. Non-Cryst. Solids **468**, 92–99 (2017)
26. M.I. Sayyed, K.M. Kaky, D.K. Gaikwad, O. Agar, U.P. Gawai, S.O. Baki, Physical, structural, optical and gamma radiation shielding properties of borate glasses containing heavy metals (Bi_2O_3/MoO_3). J. Non-Cryst. Solids **507**, 30–37 (2019)
27. S.A. Issa, H.O. Tekin, R. Elsaman, O. Kilicoglu, Y.B. Saddeek, M.I. Sayyed, Radiation shielding and mechanical properties of Al_2O_3-Na_2O-B_2O_3-Bi_2O_3 glasses using MCNPX Monte Carlo code. Mater. Chem. Phys. **223**, 209–219 (2019)
28. D. Saritha, Y. Markandeya, M. Salagram, M. Vithal, A.K. Singh, G. Bhikshamaiah, Effect of Bi_2O_3 on physical, optical and structural studies of ZnO–Bi_2O_3 –B_2O_3 glasses. J. Non-Cryst. Solids **354**, 5573–5579 (2008)
29. I. Olarinoye, Variation of effective atomic numbers of some thermoluminescence and phantom materials with photon energies. Res. J. Chem. Sci **1**(2), 64–69 (2011)
30. L. Gerward, N. Guilbert, K.B. Jensen, H. Levring, X-ray absorption in matter. Reengineering XCOM. Radiat. Phys. Chem. **60**, 23–24 (2001)
31. I.O. Olarinoye, Photon buildup factors for some tissues and phantom materials for penetration depths up to 100 MFP. J. Nucl. Res. Dev. **13**, 57–67 (2017)
32. I.O. Olarinoye, R.I. Odiaga, S. Paul, EXABCal: a program for calculating photon exposure and energy absorption buildup factors. Heliyon **5**(7), e02017 (2019)
33. E. Şakar, Ö.F. Özpolat, B. Alım, M.I. Sayyed, M. Kurudirek, Phy-X/PSD: development of a user-friendly online software for calculation of parameters relevant to radiation shielding and dosimetry. Radiat. Phys. Chem. **166**, 108496 (2020)
34. F.H. Attix, *Introduction to Radiological Physics and Radiation Dosimetry* (John Wiley & Sons, 2008).
35. A. El-Khayatt, Calculation of fast neutron removal cross-sections for some compounds and materials. Ann. Nucl. Energy **37**(2), 218–222 (2010)
36. F.A. Schmidt, Attenuation properties of concrete for shielding of neutrons of energy less than 15 MeV (No. ORNL-RSIC-26). Oak Ridge National Lab., Tenn (1970)
37. V.F. Sears, Neutron scattering lengths and cross sections. Neutron News **3**, 29–37 (1992)
38. T. Korkut, V.V. Çay, M. Sütçü, O. Gencel, Neutron radiation tests about Fe-Cr slag and natural zeolite loaded brick samples. Sci. Technol. Nucl. Ins. (2014) 190–193
39. J.F. Ziegler, M.D. Ziegler, J.P. Biersack, SRIM—the stopping and range of ions in matter. Nucl. Instrum. Methods B **268**, 1818–1823 (2010)
40. N. Elkhoshkhany, E. Syala, E. Yousef, Concentration dependence of the elastic moduli, thermal properties, and non-isothermal kinetic parameters of Yb^{3+} doped multicomponent tellurite glass system. Results Phys. **16**, 102876 (2020)
41. Y.S. Rammah, I.O. Olarinoye, F.I. El-Agawany, A. El-Adawy, A. Gamal, E.S. Yousef, Elastic moduli, photon, neutron, and proton shielding parameters of telluritebismo-vanadate (TeO_2–V_2O_5–Bi_2O_3) semiconductor glasses. Ceramics Int **46**(16), 25440–25452 (2020). https://doi.org/10.1016/j.ceramint.2020.07.014
42. I.O. Olarinoye, F.I. El-Agawany, A. El-Adawy, Y.S. Rammah, Mechanical features, alpha particles, photon, proton, and neutron interaction parameters of TeO_2–V_2O_3–MoO_3 semiconductor glasses. Ceramics Int. **46**(16), 25440–25452 (2020)
43. E. Kavaz, N. Ekinci, H.O. Tekin, M.I. Sayyed, B. Aygün, U. Perişanoğlu, Estimation of gamma radiation shielding qualification of newly developed glasses by using WinXCOM and MCNPX code. Prog. Nucl. Energy **115**, 12–20 (2019)
44. G. Lakshminarayana, I. Kebaili, M.G. Dong, M.S. Al-Buriahi, A. Dahshan, I.V. Kityk, T. Park, Estimation of gamma-rays, and fast and the thermal neutrons attenuation characteristics for bismuth tellurite and bismuth boro-tellurite glass systems. J. Mat. Sci. **55**(14), 5750–5771 (2020)